Advancing Contact Angles of Newtonian Fluids During "High" Velocity, Transient, Capillary-Driven Flow in a Parallel Plate Geometry

Harry J. Barraza, Sarat Kunapuli, and Edgar A. O'Rear*

University of Oklahoma, School of Chemical Engineering and Materials Science, Norman, Oklahoma 73019

Received: October 17, 2001; In Final Form: January 31, 2002

Advancing contact angles in the order of 70° to 80° were measured for Newtonian fluids at relatively high capillary numbers using a system of parallel glass plates. The transient height attained by the fluids between the plates was fitted to an averaged-flow Navier−Stokes model in order to indirectly estimate the value of the dynamic advancing angle. Subsequently, using a highly nonlinear approximation for the contact angle, it was possible to describe the entire relaxation phenomena during the capillary rise at low meniscus rates (e.g., high viscosity fluids), as well as at front velocities on the order of a hundred millimeters per second (e.g., low viscosity fluids). Contact angles obtained by the parallel plates method agree well with experimental observations and phenomenological correlations put forward in recent literature, but cannot be explained in terms of the proportionalities between dynamic angle and velocity predicted by the classical hydrodynamic and molecular theories in the nonwetting case.

Introduction

Spontaneous penetration of a liquid into a capillary pore initially filled with air is an old phenomenon that has gained a renewed interest for its application in oil production mechanics, composites manufacture, hydraulic engineering and other fields. To date, most experimental studies of the hydrodynamics of capillary rise are explained through a simple balance of frictional, capillary, and gravitational forces. Classical equations such as those of Washburn,[1] Lucas,[2] and Rideal,[3] are all based on the general assumption of an axisymmetric, steady-state parabolic velocity profile over a cross-section of the capillary, without any consideration to the initial transient acceleration during the first stages of penetration. Szekely[4] and Levine et al.[5] made modifications to the original Washburn's approach by introducing the appropriate momentum balance equations and considering the deviation from Poiseuille flow. However, their equations considered the existence of a single and invariable equilibrium contact angle during the entire rate of capillary rise, and made no account of inertial forces.

Berezkin[6] and Joos et al.[7] showed results on the capillary rise in cylindrical tubes under conditions where the Washburn equation did not match well with experiments. Both authors explained this anomalous behavior by empirically correlating contact angle changes with the advancing meniscus velocity. Further observations with empty and packed capillary tubes performed by Siebold et al.[8] to measure the wetting characteristics of powdered solids as probed with low viscosity hydrocarbon fluids led to the conclusion that the dynamic contact angle is always larger than its expected equilibrium value and depends strongly on the rising velocity. Hamraoui et al.,[9] on the other hand, proposed that the change in the contact angle during capillary penetration could be understood in terms of a friction coefficient, which he introduced as a correction to the original Washburn equation.

Inertia is also a major factor during the capillary rise phenomenon as well as for the change in the dynamic contact angle and the hydrodynamics near moving contact lines.[10−13] Capillary penetration tests of a fluid between parallel plates under reduced gravity were recently described by Dreyer et al.,[14−15] who dramatically showed that at an early stage of penetration the capillary rise is governed by inertial forces, leading to a linear variation of the liquid column height versus time. Kaneki et al.[16] also reports on the marked effect of gravity on the capillary penetration of ethanol in a porous-glass parallel-plates setup, and suggests the dynamic contact angle under normal gravity condition to be different from that obtained under microgravity. In normal gravity, the capillary rise up to the transition time from inertial to viscous regime also has a noticeable deviation from the parabolic correlation predicted by Washburn's equation. This effect is particularly augmented with very low viscosity fluids, as suggested from data gathered on circular capillaries by Queré[17] and Siebold et al.[8]

Several attempts have been made to introduce the inertial force into the models for capillary rise phenomena in both cylinders and parallel plates. Duarte et al.[18] uses a hydrodynamical approach containing an average of the Navier Stokes Equation (NSE) and finds an approximate solution to the nonlinear differential equation by perturbation analysis. Moshinskii[19] presents integro-differential equations that reduce to simpler solutions by way of imposing certain limiting conditions, one of which is complete wetting. Finally, there are the so-called "well-posed" models based on the instationary Navier−Stokes equations that constitute an unabridged mathematical description of the free-surface flow. Schweitzer,[20] after showing the well posedness of the equations for describing a free-surface flow with a solid boundary, also presents some arguments that favor the condition of a constant dynamic contact angle.

If the mechanism responsible for the dependence of the contact angle on the interfacial velocity, or in the whole flow field in the vicinity of the moving contact line as suggested by Blake et al.[21], is still not clearly understood; the direct measurement of the dynamic contact angle remains as an open issue. Most available methods today are limited to experimental conditions in which the wetting speed is low (i.e., Wilhelmy

* To whom correspondence should be addressed. Tel: (405) 325 5811. Fax: (405) 325 5813. E-mail: eorear@ou.edu.

10.1021/jp013849q CCC: $22.00
Published on Web 04/18/2002

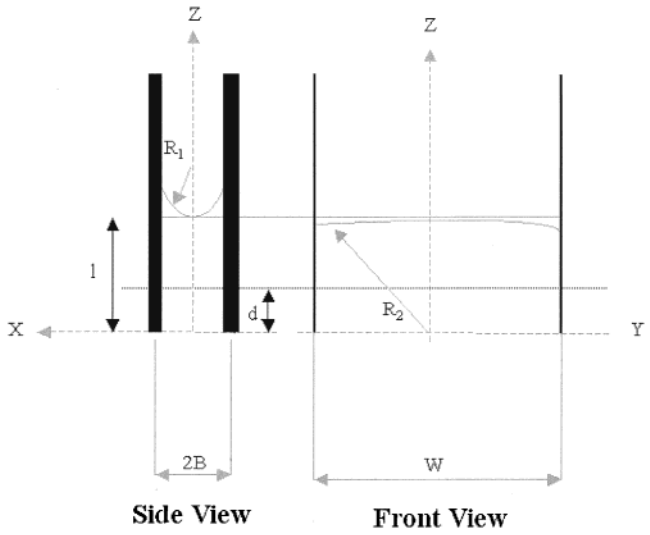

Figure 1. Parallel plate configuration with coordinate system and spatial parameters

technique), or where straight contact lines allow the use of side silhouette photography (i.e., Drop Shape Analysis). Some other recent developments comprise the use of fluorescent imaging[22] and grating shearing interference.[23] However, the accuracy of these techniques depends heavily on external factors such as fluorescent dye dispersion and laser/light alignment. On the basis of the Snell−Descartes law, Andrieu et al.[24] developed an interesting optical technique, which according to the author enables a simultaneous direct measurement of the dynamic contact angle and the velocity of the liquid front. Herein, a liquid film of less than 1 mm thick is placed over a nonwetting substrate, and given that the substrate is two-dimensionally isotropic, a hole will open up, and the dewetting velocity will vary with the dynamic contact angle. Recording the contact line and measuring its displacement with respect to a fixed objective point, it is possible to find the corresponding dynamic angle. Although, this method has an estimated accuracy of 2°, it is limited to transparent liquids and substrates, and only measures contact angles between 2° and about 30° maximum.

In this paper, we introduce an alternative method to determine the advancing contact angle from the transient height attained by a liquid during the spontaneous capillary penetration between two parallel glass plates. The basic hydrodynamical principles used are summarized in the NSE, and a simple analytical solution is found after several simplifying assumptions. Compared to existing approaches, our analysis of the parallel-plates method seems more advantageous for reasons such as the following: (i) it is based on Cartesian coordinates, which simplifies the problem and provides analytical solution from first principles; (ii) taking transient acceleration terms into account, predictions over penetration lengths at early stages of capillary flow should be more realistic; (iii) the contact angle is measured at meniscus velocities that are several orders of magnitude higher than other available techniques; that is, at maximum contact line speeds close to a hundred millimeters per second.

Theoretical

The Navier−Stokes Equation. We consider a mathematical model for capillary driven flow of a Newtonian fluid into the gap between two parallel plates. A sketch of the parallel plate geometry with key dimensions and the coordinate system employed are presented in Figure 1. The parallel plates with spacing $2B$ and width w are positioned perpendicular to the flat fluid surface, and when they are brought in contact with the fluid, the balance between surface tension, hydrostatic pressure, gravity and viscous friction creates a net force directed upward that causes the liquid to rise inside the gap. The liquid motion is governed by the time-dependent NSE, which describes the dynamic momentum balance in the fluid[25]

$$\frac{\partial \mathbf{v}}{\partial t} + (\mathbf{v}.\nabla)\mathbf{v} = -\frac{1}{\rho}\nabla p + \mathbf{f} + \frac{\mu}{\rho}\nabla^2\mathbf{v} \tag{1}$$

along with the continuity equation

$$\nabla\cdot\mathbf{v} = 0 \tag{2}$$

Herein, $\mathbf{v}$ (x, t) and p (z, t) are the velocity and pressure fields, respectively. The body force per unit fluid mass $\mathbf{f}$ is exclusively due to gravity and no other acceleration components are considered: $\mathbf{f} = -g\hat{\mathbf{k}}$. As a simplifying assumption for the mathematical model, we consider that the system is symmetrical along the length of the plates, and both plates are infinitely long in the z-direction. Using Cartesian coordinates x, y, and z, with origin on the median plane at the entrance of the channel, we postulate conditions of fully developed flow, laminar regime and uniaxial velocity component: $v_z = v_z(x, t)$. Besides taking the fluid as Newtonian, incompressible, and homogeneous, the process is regarded to be isothermal with negligible interactions between the climbing liquid and the surrounding air (i.e., no stress acts at the liquid−gas interface).

The pressure gradient can be expressed as

$$\nabla p = \frac{\Delta p}{l(t)}\hat{\mathbf{k}} \tag{3}$$

Where $l(t)$ corresponds to the liquid column height measured from the origin, and Δp is the pressure difference between the moving liquid front and the entrance to the channel. This pressure difference is made up from two contributions: the capillary pressure, which pulls the liquid upward; and the hydrostatic pressure exerted by the fluid due to gravity. The capillary pressure or dynamic Laplace pressure may be estimated from the surface tension force ($p_L = -\sigma \cos\theta/B$). A useful approximation in this case is that although the contact line is moving, the force balance equation remains valid and the pressure difference can be expressed in terms of the advancing contact angle[26,27] as

$$\Delta p = p_0 - p_L = \frac{\sigma\cos\theta_a}{B} + \rho g d \tag{4}$$

Here, the surface tension of the liquid, σ, as well as the advancing contact angle, θ_a, are considered to be time independent. B, is the channel half-width; ρ, is the density of the fluid; g, the gravity constant; and d, the depth between the free surface of the fluid in the reservoir and the entrance to the channel.

Averaging the NSE. Because the transient height $l(t)$ is a global or macroscopic quantity, a complete hydrodynamical description of the fluid motion field may not be necessary. Averaging the NSE across the liquid column may well account for the contact line velocity. Thus, integrating over a cross section away from the front, we have

$$2Bw\rho\frac{dv_{ave}}{dt} = 2Bw\frac{(p_0 - p_L)}{l(t)} + \mu w\left(\frac{\partial v_z}{\partial x}\right)_{-B}^{B} - \rho g(2Bw) \tag{5}$$

Note that after the averaging procedure the pressure term in the right-hand side of eq 1 does not change, and the relationship presented in eq 3 can be introduced without problem. For an explicit evaluation of the averaged terms calculated in eq 5, it is necessary to make an assumption concerning the form of v_z (x, t) as a function of x. With Reynolds's numbers on the order of 10 or less, we take the usual parabolic profile of laminar flow between parallel plates

$$v_z = \frac{3}{2} v_{ave}\left[1 - \left(\frac{x}{B}\right)^2\right] \quad (6)$$

Combining eqs 6 and 5 yields

$$\rho\frac{\partial v_{ave}}{\partial t} = \frac{p_o - p_L}{l(t)} - \frac{3\mu v_{ave}}{B^2} - \rho g \quad (7)$$

It is known that at very short times of capillary penetration the influence of converging flow and the so-called "fountain effect", where the liquid circulates from the system axis to the walls, are considerably active.[26] However, because the experimental apparatus has plates of length orders of magnitude greater than the inner gap, we assume that behind the fluid front most of the liquid moves in the form of stacked rigid laminae whose velocity depends on the x-position according to eq 6. Therefore, we can directly identify v_{ave} as being equal to the contact line velocity and transform eq 7 into

$$\rho\frac{d^2l}{dt^2} = \frac{(p_o - p_L)}{l} - \frac{3\mu}{B^2}\frac{dl}{dt} - \rho g \quad (8)$$

It is clear that eq 8 is different from other approximate solutions[28,29] in that a second-order derivative is introduced to account for the impulse drag effect associated with an accelerating fluid. Nondimensionalization of eq 8 can be performed using $l^* = (\rho g/\sigma)^{1/2} l$, and $\tau = [g(\rho g/\sigma)^{(1/2)}]^{(1/2)}t$ as the nondimensional height and time, respectively. Also, taking the equilibrium height attained by the system when the advancing angle is close to zero yields $l_o = p_o - p_L/\rho g$. Equation 8 transforms into

$$l^*\left(\frac{d^2l^*}{d\tau^2} + \omega\frac{dl^*}{d\tau} + 1\right) = l_0^* \quad (9)$$

Where $\omega = 3\mu/\rho B^2$ $[1/g(\sigma/\rho g)^{(1/2)}]^{(1/2)}$. The form of this nonlinear, nonhomogeneous second-order ordinary differential equation is such that an analytical solution will be composed of a linear combination of both the homogeneous solution and a "particular" solution as is presented in the Supporting Information section. The final solution after applying the corresponding boundary conditions reads

$$l = \left(d + \frac{\sigma\cos\theta_a}{\rho g B}\right) \times (1 - e^{-[(3/2)(\mu/\rho B^2) - \sqrt{((3/2)(\mu/\rho B^2))^2 - (g/2B)(Bo)^{1/2}}]t}) \quad (10)$$

Contact Angle Relaxation. Dynamic systems involving a three-phase contact line are usually divided into two distinct categories,[10] those in which the advancing (or receding) interface is driven with a constant velocity relative to the solid substrate, also called forced, or, steady displacement wetting; and those in which the interface is in nonequilibrium state, relaxing to a configuration of minimum free energy. The latter is a nonsteady process, where the triple line velocity is a decreasing function of time. Experimental observations[6] and computer simulations[30] have shown that during capillary penetration the meniscus is flat at times close to zero, which essentially means that the contact angle is $\pi/2$. The expansion of the liquid/air surface to a spherical cap of finite curvature at equilibrium results in a static meniscus with $\theta = \theta_0$. Between these two extreme values, the dynamic contact angle suffers changes originated from dissipative forces acting microscopically in the solid/liquid contact line that can be linearly correlated to the shear stress at the wall.[31]

TABLE 1: Roughness Parameters for Methanol-cleaned Glass Slides

scan size (μm)	R_a (nm)	RMS (nm)	$R_{máx}$ (nm)	n
1×1	1.6 ± 0.38	2.3 ± 0.69	17.3 ± 8.31	5
10×10	1.9 ± 0.22	2.6 ± 0.47	57.57 ± 25.22	6

Experimental Section

Materials. Model Newtonian high-viscosity liquids utilized during this study comprised: ACS certified glycerol of 99.8% purity (class IIIB), obtained from Fisher Scientific; and Brookfield silicone oil viscosity standard (500 cp). No additional information on composition and/or purity of the silicone standard was available from the manufacturer. Absolute ethanol, 200-proof, from AAPER Alcohol and Chemical Co.; and hexane from Fisher Scientific, HPLC grade (class IB), were the two low viscosity fluids used in the high meniscus velocity experiments.

Flow Cell. A cell of parallel glass plates resembling those used previously by Dreyer et al.[14] and Ngan and Dussan[32] was built with Premium microscope slides ($75 \times 25 \times 1$ mm) from Fisher Scientific. The gap thickness was controlled to three different values: 0.15, 0.30, and 0.45 mm by inserting spacers made from Premium cover glass ($30 \times 24 \times 0.15$ mm), also from Fisher Scientific, held in place by a metallic clamp. Both sides of the cell were sealed with a plastic tape, taking care that a small slot was available to vent the air and ensuring that no variations in thickness were present.

The typical cleaning procedure of the glass plates included overnight soaking in reagent grade methanol, followed by a vigorous rinsing with plenty of fresh methanol, and then final drying in a desiccator until use. Methanol/acid cleaning of microscope slides is considered a very effective method to obtain a hydrophilic surface.[33] However, in this study, we avoided any acid mixture to prevent ion-leaching induced roughening of the solid. Furthermore, individual cells were built before every experiment from randomly selected alcohol-cleaned slides in order to reduce systematic errors associated with nonuniform surface properties. Roughness parameters such as the average roughness (R_a) and roughness amplitude (RMS) of the plate's surface were measured by AFM and reported in Table 1. Flow retardation and vortices are known to occur in wall-bounded flow when the ratio of roughness to channel depth reaches a critical value of one percent.[34]

Typical Setup. A clean flow cell was carefully secured from a vertical post as shown in Figure 2; and then aligned perpendicularly to the free surface of the test liquid. Water miscible and immiscible fluids of high and low viscosity were examined (Table 2). The large reservoir containing test fluid was supported by a lab-jack, which was slowly raised until the plates were brought in contact with the liquid. Extra precaution was taken to clean and dry the container before pouring fresh glycerol to avoid any physicochemical changes due to the hygroscopic properties of glycerol. This same procedure was repeated just prior to every run with glycerol. For all the other liquids refilling was not perceived as critical, and it was

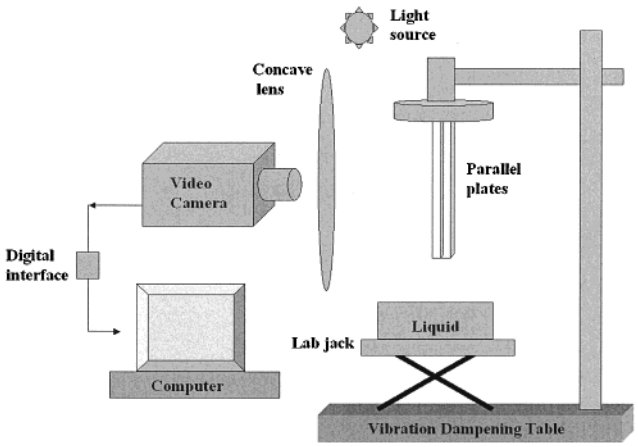

Figure 2. Experimental setup for recording transient capillary rise between parallel glass plates.

TABLE 2: Physical Properties of Test Liquids

Low Viscosity Fluids			
name	density (ρ) (Kg/m^3)	viscosity (μ) (Kg/m.s)	surface tension (σ) Kg/s^2
Ethanol	780	1.17×10^{-3}	$21.6 \times 10^{-3(\dagger)}$
Hexane	660.3	0.326×10^{-3}	$19.1 \times 10^{-3(\ddagger)}$

High Viscosity Fluids			
name	density (ρ) (Kg/m^3)	viscosity (μ) (Kg/m.s)	surface tension (σ) Kg/s^2
Glycerol	1261	954×10^{-3}	$63.4 \times 10^{-3(*)}$
Viscosity standard	$972^{(\diamond)}$	$500 \times 10^{-3(\diamond)}$	$22.2 \times 10^{-3(*)}$

All data taken from Reid[35] unless specified otherwise. (†) Reported by Queré(17). (‡) Reported by Siebold(8). (◇) Brookfield Viscosity Standard 500 data sheet. (∗) Measured at 25 °C with a Cahn DCA-322.

performed after two to three individual runs. In the experiments with high viscosity fluids, the plates were immersed to a constant depth of 3 mm as a way to increase the capillary driving pressure. Whereas for the low-viscosity fluids, the concave meniscus formed by the liquid in a Teflon beaker was barely touched with the plates to initiate the capillary rise ($d = 0$).

To determine the contact line displacement rate, a continuous video recording was made of liquid penetration into the flow cell (Figure 2). Images showed only a slight curvature of the interface along a line parallel to the plate surface. For high-viscosity liquids, a Magnavox CCD camera with a 12:1 power zoom and a concave lens were adjusted to have an optimum enlarged image covering the whole liquid penetration area and the ruler marks placed adjacent to the glass slide. Through a digital acquisition card connecting the video camera and a PC it was possible to create a digital file that was later analyzed using commercial software (Dazzle PC) having a time resolution of one second between frames. Low-viscosity liquids required better time-resolution as well as higher image quality. A SONY DSR-300 DVCAM video camera, and both a digital MEDIA 100 XR SYSTEM and a basic VHS PANASONIC AG-A750 video-editing system allowed us to acquire liquid displacement data at an interval of 30 points per second as illustrated in Figure 3. All experiments were carried out at room temperature.

Low-Rate Advancing Contact Angle. Glass squares of dimensions: $25 \times 25 \times 1$ mm, cut from the same glass slides used in the flow cells, were used to measure the advancing contact angles of all test liquids at low velocity (100 μm/s). After thorough cleaning with methanol as described above, the glass squares were hung from a microbalance in the Cahn DCA-322 system to record the force exerted by the liquid on the solid plate when it is dipped at constant velocity. Contact angles calculations using this method are based on the Wilhelmy equation.

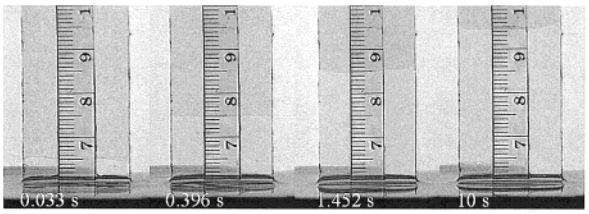

Figure 3. Transient height of ethanol in sequential video frames. Plate spacing = 0.15 mm.

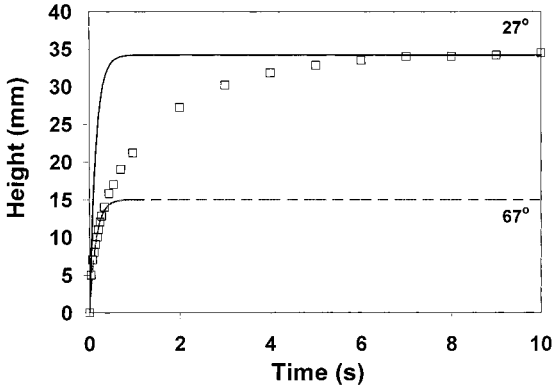

Figure 4. Constant angle model fit for ethanol at early and long penetration times. Plate spacing = 0.15 mm.

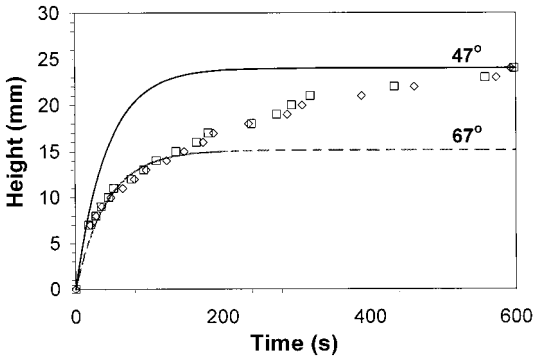

Figure 5. Constant angle model fit for viscosity standard at early and long penetration times. Plate spacing = 0.15 mm.

Results and Discussion

Constant Advancing Angle. When the opening of the parallel plate chamber contacts the surface of the liquid, fluid rises rapidly and then generally slows down as it approaches the equilibrium height. Results for ethanol are shown in Figure 4 and for the viscosity standard in Figure 5 at a gap spacing of 0.15 mm. Ethanol exhibits a very rapid initial rise followed by a gradual slowing as the liquid approaches the equilibrium height; whereas the more viscous, poorer wetting silicone oil has a similar height vs time curve shape but on a much longer time scale.

The assumption in the solution of eq 9 is that the advancing contact angle may be taken as constant during the capillary penetration experiment. This invariable contact angle model fits experimental data under two sets of conditions: early capillary rise, $\theta_{a\ (high\ velocity)}$, and close to the equilibrium, $\theta_{a\ (low\ velocity)}$. At long times of experimentation, the one-parameter equation, not surprisingly, is able to predict the advancing contact angle

at a low meniscus rate regime; that is, when the dynamic contact angle approaches the static value. It is worth noting that the dynamic contact angles at steady state probably are not at equilibrium, perhaps due to the imperceptible velocity of the meniscus in the plates (when recorded at 30 frames/second). For ethanol, an advancing contact angle of 67° fits the rapid initial rise, and the much lower value of 27° fits the low velocity portion. Under these same conditions, best fits for hexane contact angles are 70° and 33°; whereas for the viscosity standard are 67° and 47°, though the data are of poorer quality for the more viscous fluid.

Model predictions with very high contact angles are able to match the experimental transient height, at short penetration times, only up to a certain limiting point that we have designated the "critical time", (t_c). It is evident that after this point a relaxation process forces the contact angle to become smaller, which translates into higher liquid columns. By taking 90% of the plateau-height predicted by eq 10, it was possible to estimate the critical time values for all test liquids by the parameter

$$t_c = \frac{2.30258}{\left[\frac{3}{2}\frac{\mu}{\rho B^2} - \sqrt{\left(\frac{3}{2}\frac{\mu}{\rho B^2}\right)^2 - \frac{g}{2B}(Bo)^{1/2}}\right]} \qquad (11)$$

Constant advancing angles may be expected to occur at very high meniscus velocities as predicted by the present model. Hoffman[10] postulates that a constant maximum angle results whenever meniscus velocities are increased because the molecules become randomly oriented at the boundary with an attendant change in the interfacial forces, and thus the apparent contact angle. On the other hand, when the interface velocities are low enough, molecular orientations take place at the advancing liquid−solid−gas boundary. A similar plateau in the dynamic contact angle was observed for water in dry quartz ultrathin capillaries when the velocity exceeded 0.01 mm/s. Such behavior was explained by the retarded kinetics of the formation of the adsorption film in front of a rapidly moving meniscus.[36, 37]

Nonconstant Advancing Angle. The constant contact angle equation based on an averaged solution of the Navier−Stokes equation fails to describe the data during the entire course of the transient capillary rise experiments. Notwithstanding the advantages of the model presented in eq 10, it is obvious that in order to describe the complex processes that cause the changes in contact angle, we need to introduce a relaxation term into our model. A modification was based on the rationale that a small time-dependent change in the cosine of the advancing contact angle could be simply represented by a linear function with two empirical constants. These two constants may be easily evaluated using the limiting cases found with the unmodified equation. In such case the model can be described by

$$l = \left(d + \frac{\sigma(a+bt)}{\rho g B}\right) \times \left(1 - e^{-[(3/2)(\mu/\rho B^2) - \sqrt{((3/2)(\mu/\rho B^2))^2 - (g/2B)(Bo)^{1/2}}]t}\right) \qquad (12)$$

Figure 6 and Figure 7 show how expressing the cosine of the advancing contact angle in eq 10 as a linear function in time is sufficient to fit the entire capillary penetration for both high-viscosity liquids tested regardless of the cell gap-width. Perhaps this simple approximation may be valid whenever the capillary number is small, that is to say, in the region where the viscous forces are dominant. At larger meniscus velocities,

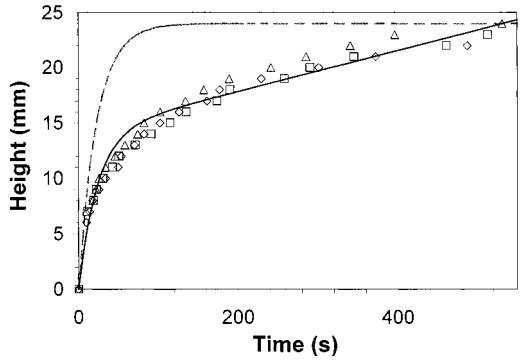

Figure 6. Transient height for glycerol. Plate spacing = 0.30 mm. Model fit with constant contact angle (dashed line). Model fit with time-dependent contact angle (solid line, equation 12).

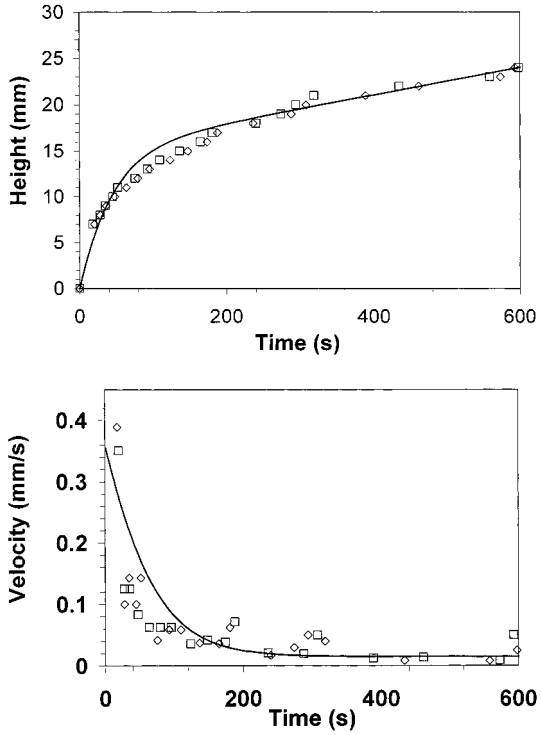

Figure 7. Transient capillary height for viscosity standard. Plate spacing 0.15 mm. (a) Model fit with time-dependent contact angle: eq 12. (b) Experimental and calculated contact line velocity.

as is the case of ethanol and hexane, the linearly modified equation seems to improve the transient height prediction up to longer times, but again the model falls short and deviates significantly from the experimental data as seen in Figure 8.

For high viscosity fluids, $\theta_{a\ (high\ velocity)}$ calculated with our model were compared to values obtained from the classical Hoffman function with the help of an expression describing the Hoffman function, proposed by Jiang et al.[38] as

$$H = \frac{\cos\theta_0 - \cos\theta_a}{\cos\theta_0 + 1} = \tanh(4.96\mathrm{Ca}^{0.702}) \qquad (13)$$

As an example, taking 45° as equilibrium contact angle, θ_0, for the viscosity standard (plate spacing: 0.15 mm); and capillary number at the maximum meniscus velocity reported in Figure 7b ($Ca = 7.8 \times 10^{-3}$), the contact angle predicted with the Hoffman function is 64.6°. A similar procedure with glycerol (plate spacing: 0.3 mm, and $Ca = 9.7 \times 10^{-3}$) gives a contact angle of 70.6°. Both values calculated with eq 13 are close to the maximum contact angles from NSE, eq 10. An exceptionally

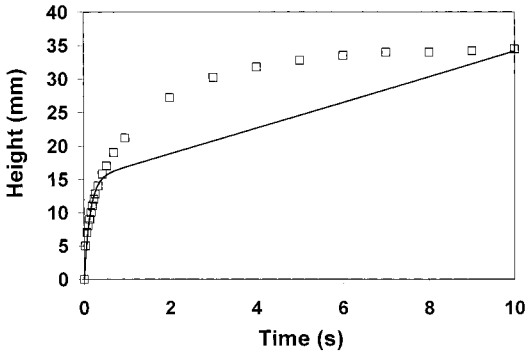

Figure 8. Model fit for ethanol transient height with nonconstant contact angle: eq 12. Plate spacing = 0.15 mm.

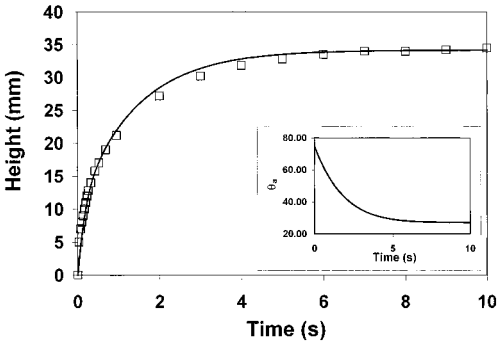

Figure 9. Model fit for ethanol transient height with nonconstant contact angle: eq 14. Plate spacing = 0.15 mm. Insert: Measured advancing contact angle.

low value of $\theta_{a\ (high\ velocity)}$ for glycerol was recorded with the smallest cell spacing ($B = 0.075$ mm). The glycerol flow front in this particular cell was always irregular and sometimes irreproducible, taking the form of a finger pattern at long penetration times. Roughness-induced instabilities were assumed to be the cause, but after considering the plate roughness magnitude presented in Table 1, this was deemed unlikely. No further consideration was then given to this phenomenon.

To improve the fit for high liquid front velocities, we put forward an operational equation for the dynamic advancing angle as a function of time that is very close to the empirical correlation presented by Newman[28] for the transient wetting of polymeric liquids; and which later was described as the relaxational spreading model.[39,40] Equation 14 describes the kinetic dependence of θ_a by analogy with the kinetic equation of a first-order reaction, that is, the rate of process ($d\cos\theta_a/dt$) is proportional to the deviation of the system from the equilibrium ($\cos\theta_0 - \cos\theta_a$). Cosine values calculated with eq 14 were directly introduced into eq 10 to obtain the theoretical transient height

$$\cos\theta_a = \cos\theta_0(1 - \psi e^{-\psi' t}) \qquad (14)$$

To evaluate the constant ψ, we considered the following boundary conditions: For $t \rightarrow \alpha$ the contact angle approaches the static value, and therefore $\cos\theta_a = \cos\theta_0$. Now, when $t \rightarrow 0$ the contact angle reaches a maximum value, "$\theta_{a(high\ velocity)}$", and the eq 14 reduces to the following: $\cos\theta_{a(high\ velocity)} = \cos\theta_0\,(1-\psi)$. Given that we know the upper and lower boundaries of the dynamic contact angle, calculating ψ is straightforward. The appropriate order of magnitude of the second constant ψ' was gauged by comparing the model predictions to the experimental measurements; and in both cases it was established that a good approximation was given by the following relation

$$\psi' = \left\{\frac{\psi}{10}\left[\frac{3}{2}\left(\frac{\mu}{\rho B^2}\right) - \sqrt{\left(\frac{3}{2}\frac{\mu}{\rho B^2}\right)^2 - g\left(\frac{\rho g}{\sigma}\right)^{1/2}}\right]\right\} \qquad (15)$$

Comparative statistics of measurements performed with the parallel plates system using the nonconstant angle model fit are reported in Table 3. Only slight differences, attributable to experimental errors, between contact angles obtained with the Wilhelmy plate technique and those angles indirectly calculated with the parallel plates at low velocities are evident. Hexane contact angles measured with the DCA322 were particularly lower than those measured in the parallel plates; which may be indicative of a higher saturation of the solid surface with hexane's vapors during the Wilhelmy experiments, as compared to a completely dry glass surface encountered by the moving liquid front in the parallel plates.

Recently published data on dynamic contact angles measured during capillary penetration experiments at high meniscus velocities substantially agree with the values of $\theta_{a\ (high\ velocity)}$ presented in Table 3. Queré[17] found a dynamic contact angle in the order of 55° for a constant capillary number of 10^{-2} in the linear penetration regime of ethanol into a glass capillary of radius 689 μm. A slightly higher value of 66° is reported by Kaneki et al.[16] as the best fit for the capillary rise of ethanol between porous glass plates under normal gravity. Siebold et al.,[8] on the other hand, photographed contact angles as high as 60° for capillary rise of alkanes in circular capillaries of radius 191 μm when the meniscus velocities were ca. 195 mm/s.

Transient height, advancing contact angle and meniscus velocity for ethanol and hexane are also depicted in Figure 9 to Figure 12. The capillary penetration of ethanol shows a much slower rate to attain the equilibrium height configuration as

TABLE 3: Contact Angles at Various Meniscus Velocities

	Glycerol			Viscosity Standard 500		
	0.15 mm	0.30 mm	0.45 mm	0.15 mm	0.30 mm	0.45 mm
$\theta_{a\ (high\ velocity)}$	61°	71°	72°	67°	66°	66°
$\theta_{a\ (low\ velocity)}$	55°	54°	55°	47°	45°	47°
$\theta_{a\ (Hoffman)}$	70.6°				64.6°	
$\theta_{a\ (Wilhelmy)}$	50.5 ± 5° ($n = 7$)				44.3 ± 3° ($n = 6$)	
	Ethanol			Hexane		
	0.15 mm	0.30 mm		0.15 mm		
$\theta_{a\ (high\ velocity)}$	75°	75°		76°		
$\theta_{a\ (low\ velocity)}$	26.7 ± 1.2° ($n = 13$)	22 ± 1.23° ($n = 5$)		32.7 ± 1.33° ($n = 6$)		
$\theta_{a\ (Wilhelmy)}$	20.1 ± 4° ($n = 6$)			11.8 ± 3° ($n = 7$)		

Note. Confidence interval of 95% shown for all measurements.

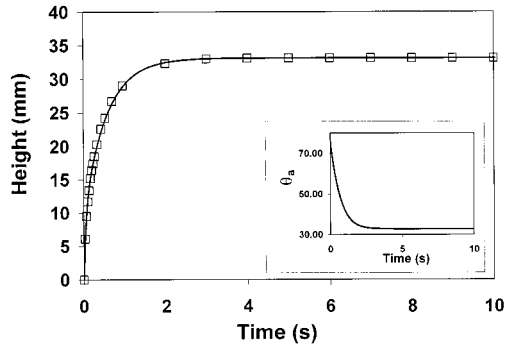

Figure 10. Model fit for hexane transient height with nonconstant contact angle: eq 14. Plate spacing = 0.15 mm. Insert: Measured advancing contact angle.

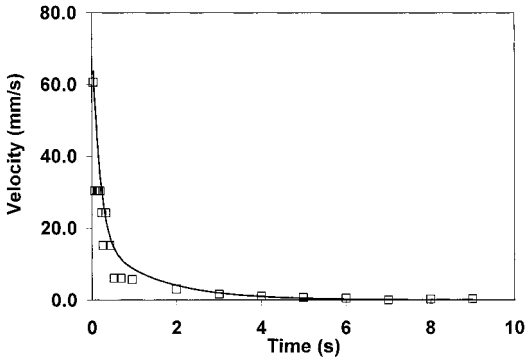

Figure 11. Experimental and calculated contact line velocity for ethanol.

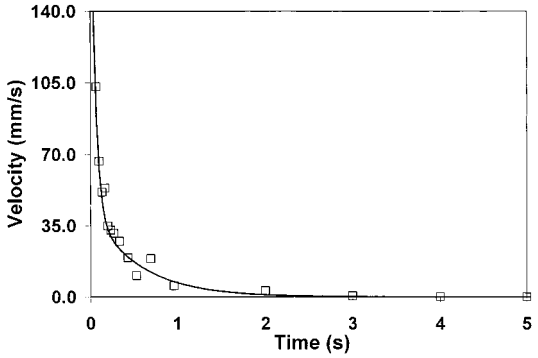

Figure 12. Experimental and calculated contact line velocity for hexane.

compared to the rate for hexane in the same 0.15 mm channel. Larger viscous resistance forces acting during ethanol rise can explain such difference; especially if we consider that both liquids have practically the same surface tension and density, but ethanol viscosity is almost four times greater than the viscosity of hexane. An order of magnitude analysis of the forces acting during the initial stages of penetration shows that distortions of the advancing interface by contributions from inertial forces can be present in our system as Weber numbers greater than the limit of 0.015 proposed by Hoffman,[10] in the case of capillary tubes, are attained by hexane and ethanol at front velocities exceeding 55 mm/s. Wider channels amplify the impulse drag effects, extending the inertial regime to longer times.

The excellent agreement between experimental and predicted values for the transient height is particularly encouraging because it means that, as expected, some of the fluid acceleration phenomena occurring at early stages of capillary penetration are accounted for in the nonconstant contact angle model.

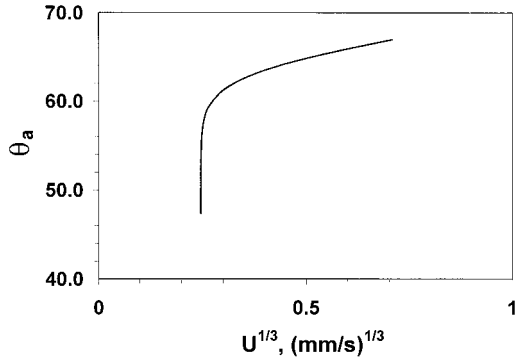

Figure 13. Dependence of the dynamic advancing contact angle on the meniscus velocity for viscosity standard re-plotted in θ_a ($U^{1/3}$) coordinates. Plate spacing = 0.15 mm.

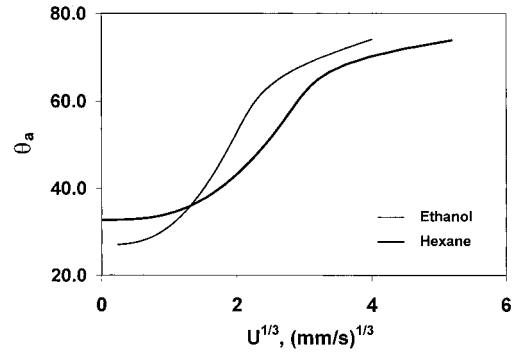

Figure 14. Dependence of the dynamic advancing contact angle on the meniscus velocity for low-viscosity fluids re-plotted in θ_a ($U^{1/3}$) coordinates. Plate spacing = 0.15 mm.

Further, we find more noteworthy the fact that using the time derivative of eq 10 along with eq 14 we are able to calculate meniscus velocities with acceptable accuracy, as evidenced in Figure 11 and Figure 12.

Two theoretical limiting cases have been proposed in the literature to determine the relation between contact line velocities, instant and equilibrium contact angles, which basically differ in the way the friction is calculated.[41] As for "dry" spreading at the macroscopic and mesoscopic scale de Gennes[42] theory suggests a qualitative dependence of the form

$$\theta_a = \left(\frac{\mu}{\sigma} U\right)^{1/3} \tag{16}$$

Figure 13 and Figure 14 show examples of contact angle data measured with the parallel plates system for high and low viscosity fluids, plotted against the meniscus velocity calculated according to eqs S7 and S8 in the Supporting Information section. Contrary to what is expected from de Gennes' theory, we found a highly nonlinear variation of the contact angle with the velocity in both cases, although some linearity is seen in regions of very low meniscus velocities. Incongruence with theory becomes more evident at capillary numbers over 10^{-3}, where the theory fails to explain the observed plateau values attained by the contact angle.

In the molecular theory developed by Blake and Haynes,[43] the dissipation associated to molecules hopping over the potential barrier represented by the contact line is believed to ultimately translate to friction resistance in flow. At the limiting condition when the solid surface is covered with an unsaturated monolayer of adsorbed liquid molecules, the molecular theory approaches the predictions of the thermodynamics of irreversible processes; and in such case, a linear dependence between

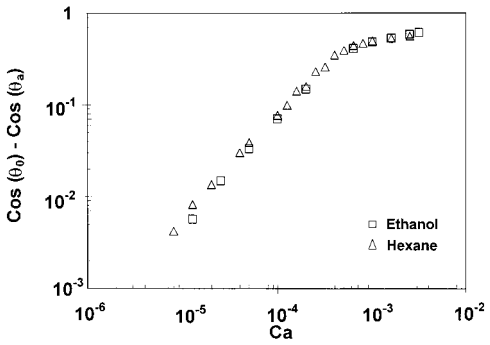

Figure 15. Wetting tension behavior of low viscosity fluids.

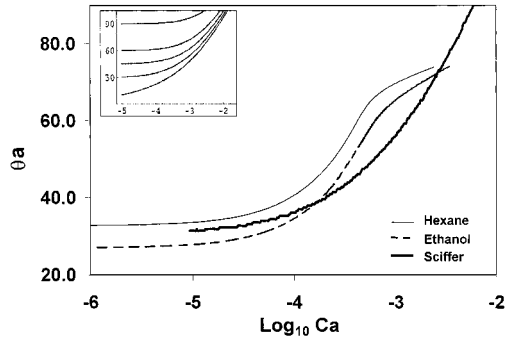

Figure 16. Measured advancing contact angles vs capillary number and comparison to Sciffer correlation ($\theta_0 = 30°$; $\beta/r_c = 100$).Insert: Effect of static contact angle $\theta_0 = 0°$, 30°, 45°, 60°, and 90°. Taken from Sciffer.[31]

spreading velocity (U) and wetting tension ($\Delta\sigma = \sigma\cos\theta_0 - \sigma\cos\theta$), described by eq 17, is believed to account for the contact angle dynamics.[44] Figure 15 shows our experimental data for ethanol and hexane re-plotted in these coordinates. Evidently, the linearity dependence exists at low capillary numbers, but again, the fact that the wetting tension ($\Delta\sigma$) reaches a plateau, indicating a practical independence of the contact angle on the velocity, cannot be explained in terms of this theoretical approach either.

$$U = L\sigma(\cos\theta_0 - \cos\theta) \tag{17}$$

Finally, contact angles measured with the parallel plates system are plotted as a function of the capillary number in Figure 16, and compared to contact angles predicted by the phenomenological correlation introduced recently by Sciffer.[31] Satisfactory agreement is found with Sciffer's predictions over similar capillary numbers and experimental conditions (e.g., $\theta_0 = 30°$ and $\beta/r_c = 100$); yet it is clear that the capillary penetration process has distinctive features that are not captured by the generalized correlation based on the linear relationship between surface tension and shear stress presented by this same author.

Conclusions

Accurate measurements of the advancing contact angles at high meniscus velocities have not been fully attained by current experimental methods. In this paper, we have presented an indirect measurement technique based on recording the transient height of a liquid column during its capillary rise in a parallel plate system, followed by a mathematical fit to an averaged-flow Navier−Stoke Equation (NSE). The resulting contact angle predictions are in good agreement with existing phenomenological models and with experimental observations at both low and relatively high capillary numbers, but deviate considerably from both hydrodynamical and molecular theories predictions. Interestingly, at the high liquid-front velocities recorded in our experiments with normal speed video the contact angle seemed to reach a maximum value, which was assumed to be constant during the early stages of penetration. Further validation of this phenomenon would explain previous observations of a linear relationship between height and time in the inertial flow regime and give firmer support to the assumptions made in our model.

Acknowledgment. The authors would like to express their gratitude to Kevin Blake from the Instructional Technology Services, University of Oklahoma; and Johnny L. Wilson, of the School of Journalism and Mass Communication, University of Oklahoma. S. Kunapuli also thanks the Undergraduate Research Experience (UROP) program of the University of Oklahoma.

Supporting Information Available: An exact solution for the second-order nonlinear ODF resulting from the analysis of the parallel plates with constant contact angle is obtained. This expression is simplified after considering the time resolution of the experiments is limited to 0.033 s. In addition, time derivatives of the transient height equation yields theoretical contact line velocities for both nonconstant angle models. This material is available free of charge via the Internet at http://pubs.acs.org.

List of Symbols

a = Model constant for variable contact angle
b = Model constant for variable contact angle
d = Depth of immersion of plates
g = Gravity acceleration
h = Meniscus height measured from the liquid free surface
l = Total liquid column height, $l = d + h$
l_0 = Equilibrium height
m_1, m_2 = Roots of the characteristic equation
p = Pressure
p_L = Dynamic Laplace pressure or capillary pressure
p_0 = Hydrostatic pressure at the entrance
t = Time
t_c = Critical time
v_{ave} = Average velocity
v_z = Velocity, z-component
w = Plate width
x,y,z = Cartesian coordinates
B = Half distance between the plates
Bo = Bond number
Ca = Capillary number
R_1, R_2 = Radii of curvature
U = Meniscus velocity
θ_a = Advancing contact angle
θ_0 = Equilibrium contact angle
μ = Viscosity
ρ = Density
σ = Surface tension
ω = Damping coefficient
τ = Nondimensional time
ψ = Model constant for variable contact angle
ψ' = Model constant for variable contact angle
$\cdots^*$ = Nondimensional quantity

References and Notes

(1) Washburn, E. *Phys. Rev.* **1921**, *17*, 273.
(2) Lucas, R. *Kolloid. Z* **1918**, *23*, 15.
(3) Rideal, E. *Philos. Mag. Ser 6* **1923**, *45*, 525.

(4) Szekely, J.; Neumann, A.; Chuang, Y. *J. Colloid Interface Sci*. **1971**, *35*, 273.
(5) Levine, S.; Lowndes, J.; Watson, E.; Neale, G. *J. Colloid Interface Sci*. **1980**, *73*, 136.
(6) Berezkin, V.; Churaev, N. *Kolloid. Z.* **1982**, *44*, 417.
(7) Joos, P.; Van Remoortere, P.; Bracke, M. *J. Colloid Interface Sci*. **1990**, *136*, 189.
(8) Siebold, A.; Nardin, M.; Schultz, J.; Walliser, A.; Oppliger, M. *Colloids Surf. A* **2000**, *161*, 81.
(9) Hamraoui, A.; Thuresson, K.; Nylander, T.; Yaminsky, V. *J. Colloid Interface Sci*. **2000**, *226*, 199.
(10) Hoffman, R. *J. Colloid Interface Sci*. **1975**, *50*, 228.
(11) Zhmud, B.; Tiberg, F.; Hallstensson, K. *J. Colloid Interface Sci.* **2000**, *228*, 263.
(12) Cox, R. *J. Fluid Mech.* **1998**, *357*, 249.
(13) Stoev, K.; Ramé, E.; Garoff, S. *Phys. Fluids.* **1999**, *11*, 3209.
(14) Dryer, M.; Delgado, A.; Rath, H.-J. *J Colloid Interface Sci.* **1994**, *163*, 158.
(15) Dryer, M.; Delgado, A.; Rath, H.-J. *Microgravity Sci. Technol.* **1993**, *4*, 203.
(16) Kaneki, Y.; Sasaki, Y.; Ishii, K.; Iguchi, M. *ISIJ International-Supplement* **2000**, *40*, S160.
(17) Queré, D., *Europhys. Lett.* **1997**, *39*, 533.
(18) Duarte, A.; Strier, D.; Zanette, D. *Am. J. Phys.* **1996**, *64*, 413.
(19) Moshinskii, A. *Kolloid. Z.* **1997**, *59*, 68.
(20) Schweitzer, B. In *Partial Differential Equations: Theory and Numerical Solutions*, Publication No. 406; Chapman & Hall: New York, 2000; p 789.
(21) Blake, T.; Bracke, M.; Shikhmurzaev, Y. *Phys. Fluids* **1999**, *11*, 1995.
(22) Johnson, M.; Schluter, R.; Bankoff, S. *Rev. Sci. Instrum.* **1997**, *68*, 4097.
(23) Shen, C.; Ruth, D. *Phys. Fluids* **1998**, *10*, 789.
(24) Andrieu, C.; Chatenay, D.; Sykes, C. *Compte Rend. Acad. Sci. Paris.* **1995**, *t320-Ser IIB*, 351.
(25) Bird, B.; Lightfoot, E.; Stewart, W. In. *Transport Phenomena*, 2nd ed.; John Wiley & Sons: New York, 2001.
(26) Van Remoortere, P. PhD Dissertation, University of Antwerpen, 1993.
(27) Friedman, S. *J Adhes. Sci. Technol*. **1999**, *13*, 1495.
(28) Newman, S. *J. Colloid Interface Sci.* **1968**, *26*, 209.
(29) Bikerman, J. In. *The Science of Adhesive Joints*; Academic Press: New York, 1961.
(30) Powell, C.; Savage, M. *Comm. Numm. Methods Eng*. **2001**, *17*, 581.
(31) Sciffer, S. *Chem. Eng. Sci.* **2000**, *55*, 5933.
(32) Ngan, C.; Dussan, E. *J. Fluid Mech.* **1982**, *118*, 27.
(33) Cras J.; Rowe-Taitt C.; Nivens, D.; Ligler, F. *Biosens. Bioelec*. **1999**, *14*, 683.
(34) Cabal, A. PhD Dissertation, University of Western Ontario, 1998.
(35) Reid, R.; Prausnitz, J.; Poling, B. In. *The Properties of Gases & Liquids*; McGraw-Hill: New York, 1988.
(36) Sobolev, V.; Churaev, N.; Velarde, M.; Zorin, Z. *J. Colloid Interface Sci*. **2000**, *222*, 51.
(37) Sobolev, V.; Churaev, N.; Velarde, M.; Zorin, Z. *Colloid J*. **2001**, *63*, 119.
(38) Jiang, T.; Oh, G.; Slattery, J. *J. Colloid Interface Sci.* **1979**, *69*, 74.
(39) Summ, B.; Raud, E. *Heat Trans−Soviet Res*. **1991**, *23*, 528.
(40) Soboleva, O.; Bogdanova, Y.; Summ, B. *Colloid J*. **2000**, *62*, 616.
(41) Cazabat, A.; Gerdes, S.; Valignat, M.; Villette, S. *Interface Sci*. **1997**, *5*, 129.
(42) De Gennes, P. *Rev. Mod. Phys.* **1985**, *57*, 827.
(43) Blake, T.; Haynes, J. *J. Colloid Interface Sci*. **1969**, *30*, 421.
(44) Summ, B.; Samsonov, V. *Colloids and Surf. A* **1999**, *160*, 63.